

Spectroscopy of Globular Clusters in NGC 4472

R.M. Sharples

Department of Physics, University of Durham, Durham DH1 3LE, England.

S.E. Zepf^{1,2,3}

Astronomy Dept, Univ. of California, Berkeley, CA, USA.

T.J. Bridges

Royal Greenwich Observatory, Cambridge, England.

D.A. Hanes²

Physics Dept, Queen's University, Kingston, Ontario, Canada.

D. Carter

Astrophysics Research Institute, Liverpool John Moores University, Byrom Street,
Liverpool, England.

K.M. Ashman

Dept. of Physics & Astronomy, University of Kansas, Lawrence, KS, USA.

and

D. Geisler

Kitt Peak National Observatory, National Optical Astronomy Observatories, Tucson, AZ,
USA.

ABSTRACT

Optical multi-slit spectra have been obtained for 47 globular clusters surrounding the brightest Virgo elliptical NGC 4472 (M49). Including data from the literature, we analyze velocities for a total sample of 57 clusters and present the first tentative evidence for kinematic differences between the red and

¹Hubble Fellow

²Visiting Astronomer, William Herschel Telescope. The WHT is operated on the island of La Palma by the Isaac Newton Group in the Spanish Observatorio del Roque de los Muchachos of the Instituto de Astrofísica de Canarias.

³present address: Astronomy Dept, Yale University, New Haven, CT, USA.

blue cluster populations which make up the bimodal colour distribution of this galaxy. The redder clusters are more centrally concentrated and have a velocity dispersion of 240 kms^{-1} compared with 320 kms^{-1} for the blue clusters. The origin of this difference appears to be a larger component of systematic rotation in the blue cluster system. The larger rotation in the more extended blue cluster system is indicative of efficient angular momentum transport, as provided by galaxy mergers. Masses estimated from the globular cluster velocities are consistent with the mass distribution estimated from X-ray data, and indicate that the M/L_B rises to $50 \text{ M}/\text{L}_\odot$ at 2.5 R_e .

Subject headings: globular clusters: kinematics, metallicities; galaxies: masses, M/L ratios

1. Introduction

The study of extragalactic globular cluster systems can provide important clues to the formation history of their host galaxies. This is particularly true for elliptical galaxies for which there are two currently popular paradigms. One paradigm is the standard monolithic collapse model in which elliptical galaxies form in a single burst of star formation at high redshift (e.g. Arimoto & Yohii 1987). In contrast, hierarchical structure formation theories predict that spheroidal galaxies form continuously through a sequence of galaxy mergers (e.g. Cole *et al.* 1994; Kauffmann 1996). Ashman & Zepf (1992) explored the properties of globular clusters in models in which elliptical galaxies are the products of the mergers of spiral galaxies, and showed that the greater specific frequency of globular clusters around ellipticals relative to spirals could be explained if globular clusters form during the mergers. They also predicted that elliptical galaxies formed by mergers will have two or more populations of globular clusters - a metal-poor population associated with the progenitor spirals, and a metal-rich population formed during the merger. In contrast, monolithic collapse models naturally produce unimodal metallicity distributions. The discovery that the globular cluster systems of several elliptical galaxies have bimodal colour (and by implication metallicity) distributions (Zepf & Ashman 1993; Whitmore *et al.* 1995; Geisler *et al.* 1996) provides strong support for the merger model. Geisler *et al.* (1996) and Lee *et al.* (1998) also show that the red (metal-rich) cluster population is more centrally concentrated than the blue (metal-poor) population, as predicted by Ashman & Zepf (1992).

Recently, an alternative view has been presented by Forbes *et al.* (1997), who suggest that the bimodal color distributions may not be due to mergers, but to a multi-phase single

collapse. Although the primary physical mechanism known to produce distinct formation episodes is mergers, it is important to attempt to distinguish between these competing models for the formation of globular cluster systems and their host elliptical galaxies. The kinematics of globular cluster systems may offer such a test of these models. In the multi-phase collapse picture, angular momentum conservation requires that the spatially concentrated metal-rich population rotates more rapidly than the extended metal-poor population. In contrast, simulations of merger models indicate that mergers typically provide an efficient means of angular momentum transfer, and that the central regions have specific angular momentum that is lower than the outer regions (Hernquist 1993; Heyl, Hernquist and Spergel 1996).

Studies of the kinematics of globular cluster systems therefore provide important constraints on the formation history of elliptical galaxies. They also provide useful probes of the mass distribution of elliptical galaxies at radii larger than can be reached by studies of the integrated light. The extended nature of globular cluster systems allows the dynamical mass determined from their velocities to be compared at similar radii to masses determined through studies of the hot X-ray gas. A recent example is the study of the M87 globular cluster system by Cohen & Ryzhov (1997), who find that a rising mass-to-light ratio is required out to radii of $\sim 3R_e$, in agreement with X-ray mass determinations. However, M87 occupies a privileged position at the center of the Virgo cluster, so it is critical to test whether the rising mass-to-light ratio, and the agreement with X-ray masses, is true for more typical cluster elliptical galaxies.

In this paper we present a spectroscopic study of the globular cluster system of the elliptical galaxy NGC 4472 (M49). This is the brightest elliptical galaxy in the Virgo cluster and has been the subject of a detailed photometric study by Geisler *et al.* (1996). The only previously published spectroscopic data for the NGC 4472 globular cluster population is by Mould *et al.* (1990) who presented velocities and line strengths for 26 clusters.

The outline of our paper is as follows: Section 2 discusses the sample selection together with our observations and data reduction; Section 3 discusses the kinematics of the metal-rich and metal-poor populations in the context of the merger model, and analyses the implications for the overall M/L ratio in NGC 4472. Finally, we present our conclusions in Section 4.

2. Observations and Data Reduction

Geisler *et al.* (1996) have made a deep ($R \sim 25$) photometric study of the globular cluster system surrounding NGC 4472 in the integrated Washington CT₁ system. They showed that the colour distribution was clearly bimodal and could be well-fit by two Gaussians with peaks at $C - T_1 = 1.32$, and $C - T_1 = 1.81$, corresponding to metallicities of $[\text{Fe}/\text{H}] = -1.3$ and -0.1 . We selected our sample for spectroscopic study from a preliminary version of the Geisler *et al.* (1996) catalogue. In order to avoid any biases in the spectroscopic cluster sample, particularly with regard to the presence of any young cluster population, we have applied only a very broad colour cut of $0.5 < C - T_1 < 2.2$ together with a magnitude cut of $19.5 \leq V \leq 22.5$ to the original catalogue, where $V \simeq T_1 + 0.5$ (Geisler 1996). The colour distribution of this sample is shown in Fig. 1. Because the catalogues are incomplete near the bright central parts of the galaxy, the multi-slit masks were offset along the major axis of the galaxy by $\sim 3'$ in order to maximise the spatial and spectral coverage of the samples.

Spectroscopic observations of 79 cluster candidates were obtained with the Low Dispersion Survey Spectrograph (Allington-Smith *et al.* 1994) on the 4.2m William Herschel Telescope in April 1994. Further details of the observing setup are given in Table 1 and in Bridges *et al.* (1997). Dome and twilight flats were taken at the beginning and end of each night, and the spectra were wavelength calibrated using frequent CuAr arcs. Long-slit spectra of the Galactic globular clusters M92 (NGC 6341; $[\text{Fe}/\text{H}] = -2.24$), M13 (NGC 6205; $[\text{Fe}/\text{H}] = -1.65$) & NGC 6356 ($[\text{Fe}/\text{H}] = -0.54$), and the radial velocity standards HD194071 (G8III) & HD132737 (K0III) were taken for velocity and metallicity calibration. Data reduction for the first mask followed closely the procedures detailed in Bridges *et al.* (1997) using the LEXT (Allington-Smith *et al.* 1994) software package. A 3rd order polynomial fit to the arc spectra gave residuals $\sim 0.13\text{\AA}$ (8 kms^{-1}) and the spectra were rebinned to linear and logarithmic wavelength scales over the wavelength range $3800 - 6000\text{\AA}$ with a bin size of 2.0\AA . The spectra were then optimally extracted and sky subtracted, using linear fits for the background sky.

For the other two masks a slightly different procedure was followed. Rather than adjust the individual multi-slit lengths to fill the available mask dimensions, a fixed-length multi-slit of $8''$ was adopted and the targets were nodded up and down the slits by $\pm 2''.5$ on consecutive exposures. This procedure allowed us to substantially increase the number of objects observed per mask and, by differencing pairs of exposures to subtract the sky background, removed some of the systematic effects due to flatfielding and irregularities in the slit profiles during this crucial stage. Comparison of spectra for objects observed on more than one mask (§2.1) indicated that this technique does not degrade the S/N achieved

and substantially increased the efficiency of our observations.

2.1. Radial Velocities and Confirmed Globular Clusters

Radial velocities were obtained by cross correlating with the template spectra of M13, M92, NGC 6356, HD132737 and HD194071, and forming a weighted average of the results after rejecting poor matches (normalised correlation amplitudes < 0.15). Velocities for the template clusters were taken from Hesser *et al.* (1986). Cross-correlation of spectra from the twilight sky frames indicated an rms velocity uncertainty of 37 kms^{-1} for high S/N data; this was added in quadrature to the scatter between templates to give the final velocity errors in Table 2. Eleven objects were measured on more than one mask and have an rms velocity difference of 54 kms^{-1} , which is consistent with the estimated velocity errors. Table 2 contains positions, colour and magnitudes for 79 cluster candidates for which spectra were obtained, together with velocities and velocity errors for 55 objects with reliable cross-correlation results (generally against 3 or more templates). The astrometric solution was obtained from a fit to 43 secondary standards distributed across the field and the relative positions should be good to $\pm 0''.3$. The colour distribution of the 55 objects with radial velocities is shown in Figure 2.

A histogram of the radial velocities of these 55 objects is given in Figure 3. Following Mould *et al.* (1990) we take the velocity range $300 < V_{he} < 2000 \text{ kms}^{-1}$ as representative of globular clusters belonging to NGC 4472 which has a recession velocity of 961 kms^{-1} (Sandage & Tammann 1981); the 47 objects in this range have a mean velocity of $943 \pm 38 \text{ kms}^{-1}$ and a velocity dispersion of 258 kms^{-1} . Assuming $\sigma = 110 \text{ kms}^{-1}$ for halo subdwarfs (Mould *et al.* 1990), the lowest velocity object in our cluster sample (2163) has a 4% chance of belonging to the NGC 4472 system and only 0.02% of being a Galactic star; the highest velocity object excluded (7731) has a 17% chance of being a Galactic star and only 0.2% chance of belonging to the NGC 4472 system. Including or excluding these objects from the cluster sample gives a velocity dispersion in the range $248 - 279 \text{ kms}^{-1}$.

3. Results

The only previous spectroscopic study of the NGC 4472 globular cluster system is that of Mould *et al.* (1990), who obtained spectra for 54 candidates from which they identified 26 clusters. The contamination by foreground stars and background stars in their study (49%) is higher than that obtained here (15%), presumably due to the magnitude and colour range

adopted. Thirteen objects in Table 2 are in common with the Mould *et al.* (1990) sample; for twelve of these the radial velocity measurements are in good agreement, with a mean difference of -2 kms^{-1} and a dispersion of 79 kms^{-1} . The remaining object (5090) has a velocity of 582 kms^{-1} in Table 2 and 959 kms^{-1} in Mould *et al.* (1990); although we only have one spectrum of this object, there are good cross-correlations with all of the templates and it seems likely that the source of the discrepancy is a mis-identification.

Table 3 contains data for the combined sample of 57 clusters. The mean velocity error for the overlap sample from our measurements is 46 kms^{-1} , so we have adopted a typical 1σ error of $\sqrt{(79^2 - 46^2)} = 65 \text{ kms}^{-1}$ for those clusters with velocities from Mould *et al.* (1990). Where clusters have velocities available from our LDSS-2 data, we list these in preference because of their smaller formal errors; however, the results presented below do not change significantly if instead the two datasets are averaged. Also indicated in this table is the angular distance of each cluster from the centre of NGC 4472 (taken as RA=12 27 15.0 Dec=+08 16 45 (1950)) and the projected distance along the major axis of the elliptical isophotes of the galaxy (taken as PA=162°; Sandage & Tamman 1981). The [Fe/H] values are taken from Geisler *et al.* (1996).

3.1. Kinematic Properties

One of the most important characteristics of the NGC 4472 globular cluster system is the clear bimodal nature of its colour (metallicity) distribution. Geisler *et al.* (1996) have already demonstrated structural differences between the metal-rich and metal-poor populations, with the metal-rich clusters being significantly more concentrated to the centre of NGC 4472 than their metal-poor counterparts. The primary goal of our study was therefore to search for any kinematic differences between the metal-rich and metal-poor globular cluster populations.

In order to divide the sample, we have run a KMM mixture-modelling test (Ashman *et al.* 1994) which indicates that the most probable boundary between the metal-rich and metal-poor clusters is at $C-T_1=1.625$ or $[\text{Fe}/\text{H}]=-0.57$ (c.f. Fig. 1). Fig. 4 shows the velocity histograms for the 57 clusters in Table 3 divided in this way. The two distributions do indeed appear to be different with the metal-rich clusters having a lower velocity dispersion; an F-test rejects the hypothesis that the two populations have the same dispersion at the 86% confidence level. Although only tentative given the current sample size, this is a potentially powerful result, and would represent the first detection of a velocity dispersion difference in a bimodal globular cluster system. In particular it reinforces the claim that the metal-rich and metal-poor populations are distinct (e.g. Zepf & Ashman 1993, Geisler

et al. 1996). We investigate the possible origins of these differences further below.

3.1.1. Rotation Velocity

One of the key observations for testing galaxy formation models is the amount of systematic rotation in globular cluster subsystems. Since mergers are believed to be effective in transporting angular momentum outwards, this provides a mechanism by which the resulting cluster population can form a dynamical system primarily supported by anisotropy rather than rotation. This natural route to hot, slowly rotating dynamical systems (at least near the centre) does not arise in a (modified) monolithic collapse picture where dissipation is included to account for the concentrated distribution of metal-rich clusters compared to metal-poor clusters. Figure 5 shows the velocities of the globular clusters in Table 3 plotted against their radial distance projected along the major axis of NGC 4472. Formally, the least squares fits to the metal-poor and metal-rich subpopulations are $0.57 \pm 0.39 \text{ kms}^{-1}/\text{arcsec}$ (Spearman rank correlation coefficient 0.26) and $0.10 \pm 0.31 \text{ kms}^{-1}/\text{arcsec}$ (correlation coefficient -0.07). However, this method assumes that the line of nodes of the cluster system is the same as that of the galaxy, which may not be the case if the system has undergone a major merger.

To constrain the rotation amplitude of the whole cluster system more generally, we have fitted a function of the form

$$V(r) = V_{\text{rot}} \sin(\theta - \theta_0) + V_o \quad (1)$$

to the radial velocity and position angle data using a non-linear least-squares algorithm. The resulting amplitude of rotation V_{rot} is $85 \pm 35 \text{ kms}^{-1}$ at position angle $\theta_0 = 125 \text{ deg} \pm 30 \text{ deg}$, in the same sense as the rotation of the stellar component (NE approaching, SE receding). This is consistent with, but somewhat smaller than the value of 113 kms^{-1} found by Mould *et al.* (1990) using a smaller sample. To check the reality of this result we have repeated the fit after randomizing the position angles of the clusters; in 50 trials, 12% of the fits had a rotation amplitude greater than or equal to 85 kms^{-1} , giving a confidence level of 88% that the detected rotation is real. Since the significance of this result is not very large, we have attempted to put an upper bound on the rotation of the whole cluster system using Monte-Carlo simulations. By generating artificial samples with the same positional angle distribution as the data, but with velocities selected from a fixed velocity amplitude chosen to lie in the range from $50 - 250 \text{ kms}^{-1}$ and a fixed dispersion of 258 kms^{-1} , we can put an upper limit on V_{rot} of 150 kms^{-1} at the 95% confidence level. As noted by Mould *et al.* (1990), one of their clusters (# 19) has a significantly larger radial velocity than

any of the other clusters and should probably be excluded from the fit; Table 4 shows the corresponding values excluding this cluster.

Figure 6 shows the results obtained when these fits are made to the metal-rich and metal-poor subsamples separately. Although the sample size is small, there is evidence that the metal-poor (blue) clusters rotate faster than the metal-rich (red) clusters. This is opposite to what is expected in a conventional collapse picture, where the natural outcome is an old, slowly rotating, metal-poor halo population of clusters, surrounding a younger, more concentrated, population of metal-rich clusters which has spun-up due to conservation of angular momentum (c.f. the situation in our own Galaxy). Mergers however provide a natural mechanism for transfer of angular momentum from the metal-rich to the metal-poor clusters. There is also a hint in Table 4 that the rotation axis for the metal-rich clusters may not be the same as that of the stellar component ($PA = 162$ deg) and the blue clusters. This is also what might be expected in the merger picture, although given the small number of clusters, the statistical significance is weak.

3.2. Velocity Dispersion

Figure 7 illustrates the velocity dispersion profile of the globular cluster system of NGC 4472. Flat rotation curves with the amplitudes given in Table 4 have been subtracted from the blue and red populations independently. The open circles show the robust estimators of velocity dispersion and errors using the ROSTAT code (Bird & Beers 1993) with all the data included; the open squares show the effects of removing cluster #19 from the sample (note that although cluster #19 is only in the final radial bin, removing it from the sample affects all the points, since the rotation velocity correction is also different c.f. Table 4). Also plotted are the stellar velocity dispersion data for the integrated light of the galaxy from Fisher *et al.* (1995). The clusters appear to form a hotter dynamical population than the halo stars, but unlike the case of M87 (Cohen & Ryzhov 1997), the dispersion profile does not increase with radius. Because the clusters and stars are known to have different structural profiles (Lee *et al.* 1998), they may still, of course, be in dynamical equilibrium with a single halo mass distribution.

3.3. Mass-to-Light Ratio

The halo mass distribution of elliptical galaxies is poorly known because of the lack of easily observed tracers such as cold HI gas. Globular clusters provide a potentially

very important probe of the outer regions of ellipticals (e.g. Cohen & Ryzhov 1997) to complement the use of planetary nebulae (Ciardullo *et al.* 1993) and X-ray gas (Nulson & Böhringer 1995). Fig 8 shows the integrated mass distribution for NGC 4472. The solid points are X-ray estimates from Irwin & Sarazin (1996). Open circles show the projected mass estimator of Heisler *et al.* (1985) applied to our globular cluster sample assuming isotropic orbits and an extended mass distribution. The assumption of a point mass distribution would decrease the projected mass estimator by a factor ~ 2 , but this assumption is clearly inconsistent with the extended mass profile implied by the X-ray data. More likely, the slightly higher mass estimate from the globular cluster data reflects a tangential anisotropy in the orbits, and there is some evidence to support this in our rotation analysis of the clusters. Correcting the velocities for our best-fit rotation solution decreases the projected mass estimator by $\sim 20\%$. More importantly, any tendency for the cluster populations to have *radially* anisotropic orbits, as might be expected in a monolithic collapse scenario, would increase the projected mass estimator even further above that derived from the X-ray gas.

We have calculated the M/L_B ratio using a standard B-band growth curve from the RC3 (de Vaucouleurs *et al.* 1991), assuming a distance to Virgo of 16 Mpc. At a projected distance of $\sim 2.5 R_e$ ($4'$), the projected mass estimator gives $M \approx 2.5 \cdot 10^{12} M_\odot$ which implies $M/L_B \approx 50 M/L_\odot$. This may be compared with a value of $M/L_B \approx 7 M/L_\odot$ derived by Saglia *et al.* (1993) from the stellar kinematics of the integrated light. Clearly these kinematic studies indicate that the M/L ratio is increasing rapidly with radius, and support the conclusion from X-ray measurements that NGC 4472 has an extended dark matter distribution similar to (although possibly not as extreme as) that seen in M87.

4. Conclusions

We have made a detailed spectroscopic study of the globular cluster system of NGC 4472, and have more than doubled the number of confirmed clusters to 57. Whilst this remains a statistically small sample, the data show several interesting properties when combined with the accurate colour/metallicity data from Geisler *et al.* (1996). When the complete sample is divided into a metal-rich (47%) and a metal-poor (53%) subset on the basis of their bimodal colour histogram, the metal-poor subset appears to have a broader distribution of velocities. We have investigated this further, and conclude that the most likely cause is a higher mean level of rotation in the metal-poor cluster system, which is consistent with that of the underlying stellar halo in amplitude and position angle (but with a much higher specific angular momentum). The metal-rich clusters on the other

hand show only weak evidence for any rotation, and about an axis which is tilted $\sim 50^\circ$ from that of the other components. These results are qualitatively in agreement with the predictions of a model in which the metal-rich clusters are formed during the merger of two massive gas-rich galaxies, each with its own old metal-poor cluster population. The cluster system of NGC 4472 forms a dynamically hotter population than the stellar halo, but is consistent with being in dynamical equilibrium with the halo potential defined by the hot X-ray emitting plasma, and supports the presence of a dark $\sim 10^{12} M_\odot$ halo in this giant elliptical galaxy.

We thank Ken Freeman for useful discussions, Karl Glazebrook for his updates to the Unix version of the LEXT data reduction package, and Jeremy Mould for providing finding charts to identify previously observed clusters. SEZ acknowledges receipt of a Hubble Fellowship. DAH would like to acknowledge support through an Operating Grant awarded by the Natural Sciences and Engineering Research Council of Canada. This work was undertaken with the support of NATO Collaborative Research Grant No. 941223 and is supported in part by NASA through grant No. GO-06699.01-95A (to D.G.) from the Space Telescope Science Institute, which is operated by the Association of Universities for Research in Astronomy, Inc., under NASA contract NAS5-26555.

Table 1. Observing Log.

Dates	April 11-14, 1994
Telescope/Instrument	4.2m WHT/LDSS-2
Dispersion (Resolution)	2.4 Å/pixel (6 Å FWHM)
Detector	1024 ² TEK CCD
Wavelength Coverage (max)	3800–6000 Å
Seeing	1–2"
Exposure time (Mask #1/#2/#3)	3.0/3.5/3.5 hr
Number of Objects (Mask #1/#2/#3)	21/38/38

Table 2. Velocities of globular cluster candidates in NGC 4472. Successive columns give ID, T1 magnitude, C-T1 colour (all from Geisler *et al.* 1996), heliocentric velocity, velocity error, RA(1950) and Dec(1950).

ID	T1	C-T1	V(he)	Err	RA(1950)	Dec(1950)	ID	T1	C-T1	V(he)	Err	RA(1950)	Dec(1950)
1407	21.89	1.28	-8	44	12 27 04.91	8 12 46.4	5263	19.91	0.77	-88	40	12 27 03.22	8 17 30.0
1483	20.75	1.56			12 27 12.94	8 12 57.8	5323	20.33	0.82			12 27 16.29	8 17 33.8
1518	19.25	1.85	1050	36	12 27 07.89	8 13 00.5	5511	21.17	1.74			12 27 17.31	8 17 44.7
1650	20.85	1.95			12 27 23.29	8 13 13.4	5561	20.82	1.39	903	48	12 26 56.84	8 17 48.3
1712	20.36	1.34	1144	40	12 27 07.54	8 13 18.9	5629	21.09	1.36	522	52	12 27 11.90	8 17 52.2
2031	20.71	1.37			12 27 15.12	8 13 46.3	5673	21.73	1.25			12 27 20.81	8 17 54.2
2045	20.94	1.77	857	54	12 27 06.50	8 13 47.7	5943	21.07	1.56			12 27 11.46	8 18 11.6
2140	20.45	1.80	730	53	12 27 21.64	8 13 55.3	6164	19.79	1.65	426	30	12 27 12.25	8 18 27.1
2163	20.15	2.01	402	43	12 27 23.34	8 13 57.6	6284	19.44	1.57	569	54	12 27 25.39	8 18 36.8
2178	21.51	1.19			12 27 04.82	8 13 59.0	6294	21.02	1.64	1034	84	12 27 01.30	8 18 37.7
2306	20.35	1.62			12 27 25.13	8 14 09.0	6427	21.11	1.79	1141	50	12 27 12.47	8 18 47.5
2341	20.76	1.91	1001	68	12 27 00.21	8 14 12.9	6520	20.06	1.86	607	57	12 27 16.75	8 18 53.5
2406	20.84	2.03	1244	70	12 27 13.23	8 14 18.4	6564	20.03	1.34	1077	31	12 27 10.77	8 18 57.2
2482	21.58	2.08	767	56	12 27 10.16	8 14 24.6	6696	20.08	1.59	550	52	12 27 21.45	8 19 08.5
2543	20.27	1.36	1199	48	12 27 20.33	8 14 29.3	6721	21.09	1.73	1180	45	12 27 07.36	8 19 10.5
2569	20.12	1.89	1056	46	12 27 11.32	8 14 31.7	6872	20.15	1.46	870	41	12 27 09.21	8 19 20.7
2634	19.70	1.56	1014	57	12 27 07.08	8 14 37.9	6989	20.61	1.75	1071	50	12 27 21.98	8 19 30.5
2679	21.38	1.59			12 27 19.00	8 14 41.5	7174	21.01	1.51			12 27 20.43	8 19 46.3
2757	19.62	1.45	-79	37	12 27 08.35	8 14 47.2	7197	20.94	1.50	782	50	12 27 08.44	8 19 48.2
2860	20.27	1.21			12 27 22.00	8 14 52.5	7340	20.91	1.77	1308	124	12 27 17.39	8 19 59.0
3119	20.78	1.74	11068	50	12 27 15.44	8 15 09.9	7399	20.35	1.40	1005	44	12 27 01.33	8 20 05.1
3150	21.40	1.79	952	42	12 27 05.95	8 15 12.1	7458	20.75	1.84	807	57	12 27 12.23	8 20 08.6
3323	21.29	1.60	12321	50	12 27 26.82	8 15 22.8	7615	21.13	1.68			12 27 11.53	8 20 20.2
3412	19.83	0.72	-203	38	12 27 09.07	8 15 30.1	7659	19.87	1.34	1571	56	12 27 10.54	8 20 24.0
3592	20.15	0.79			12 27 16.91	8 15 41.4	7731	19.55	0.82	151	48	12 27 19.33	8 20 30.2
3628	21.22	1.90	1008	49	12 27 00.59	8 15 43.9	7784	19.20	1.52	868	51	12 27 23.22	8 20 34.4
3789	19.52	1.70			12 27 30.22	8 15 53.6	7894	21.61	1.73	730	81	12 27 01.99	8 20 37.2
3808	20.35	1.83	832	35	12 27 06.60	8 15 54.5	7938	20.92	1.44	1251	50	12 27 11.90	8 20 47.7
3865	21.60	0.80			12 27 02.92	8 16 17.2	8090	20.51	1.46	903	66	12 27 13.14	8 21 00.9
3980	21.15	1.28	1112	45	12 27 03.05	8 16 05.4	8165	20.22	1.39	1027	47	12 27 23.57	8 21 06.8
4017	20.92	1.42			12 27 25.05	8 16 07.8	8228	21.48	1.77			12 27 09.19	8 21 11.9
4168	20.36	1.68	1384	44	12 27 07.64	8 16 19.4	8353	20.03	1.98	928	40	12 27 08.71	8 21 22.8
4386	19.83	1.94	1197	33	12 27 19.16	8 16 34.7	8384	21.39	1.41	768	54	12 27 15.30	8 21 24.4
4513	20.10	1.85	908	80	12 27 09.77	8 16 42.7	8516	21.82	2.01			12 27 05.28	8 21 36.6
4542	20.62	0.68			12 27 22.64	8 16 44.5	8665	19.60	0.69	-218	35	12 27 11.86	8 21 50.6
4731	19.96	1.43	698	57	12 27 09.55	8 16 58.1	8890	20.41	1.88	870	65	12 27 15.77	8 22 14.0
4780	19.52	1.95	971	45	12 27 20.79	8 17 00.9	8909	21.91	1.40			12 27 02.41	8 22 15.3
4959	21.38	1.33	1449	44	12 27 23.05	8 17 11.9	9009	21.28	1.99			12 27 12.26	8 22 24.1
5090	19.83	1.61	582	46	12 27 09.43	8 17 20.2	9228	21.01	1.61			12 27 09.08	8 22 50.5
5112	20.35	0.89			12 27 16.37	8 17 21.4							

Table 3. NGC 4472 confirmed globular clusters. Successive columns give ID, T1 magnitude, C-T1 colour, heliocentric velocity, velocity error, galactocentric radius, projected radius along the major axis, [Fe/H], RA(1950), Dec(1950) and the identification in Table III of Mould *et al.* (1990).

ID	T1	C-T1	V(he)	Err	r ($''$)	r_{maj} ($''$)	[Fe/H]	RA(1950)	Dec(1950)	Other ID
1518	19.25	1.85	1050	36	248	181	0.0	12 27 07.89	8 13 00.5	234
1712	20.36	1.34	1144	40	234	162	-1.2	12 27 07.54	8 13 18.9	
2031	20.71	1.37	1352 ¹	65	178	170	-1.2	12 27 15.12	8 13 46.3	142
2045	20.94	1.77	857	54	217	129	-0.2	12 27 06.50	8 13 47.7	
2060	20.62	1.29	1108 ^a	65	212	132	-1.3	12 27 07.15	8 13 48.3	243
2140	20.45	1.80	730	53	196	192	-0.2	12 27 21.64	8 13 55.3	
2163	20.15	2.01	402	43	208	197	0.3	12 27 23.34	8 13 57.6	
2341	20.76	1.91	1001	68	267	77	0.1	12 27 00.21	8 14 12.9	
2406	20.84	2.03	1244	70	149	131	0.4	12 27 13.23	8 14 18.4	
2482	21.58	2.08	767	56	157	111	0.5	12 27 10.16	8 14 24.6	
2528	20.34	1.46	654 ^a	65	139	138	-1.0	12 27 16.79	8 14 28.2	118
2543	20.27	1.36	1199	48	157	153	-1.2	12 27 20.33	8 14 29.3	90
2569	20.12	1.89	1056	46	144	110	0.1	12 27 11.32	8 14 31.7	196
2634	19.70	1.56	1014	57	173	84	-0.7	12 27 07.08	8 14 37.9	245
3150	21.40	1.79	952	42	163	46	-0.2	12 27 05.95	8 15 12.1	
3307	20.25	1.53	1790 ^a	65	237	148	-0.8	12 27 29.92	8 15 21.3	19
3628	21.22	1.90	1008	49	222	-8	0.1	12 27 00.59	8 15 43.9	
3808	20.35	1.83	832	35	134	9	-0.1	12 27 06.60	8 15 54.5	
3980	21.15	1.28	1112	45	182	-17	-1.4	12 27 03.05	8 16 05.4	
4168	20.36	1.68	1384	44	112	-10	-0.4	12 27 07.64	8 16 19.4	
4386	19.83	1.94	1197	33	63	29	0.2	12 27 19.16	8 16 34.7	
4513	20.10	1.85	908	80	78	-22	0.0	12 27 09.77	8 16 42.7	
4731	19.96	1.43	698	57	82	-38	-1.0	12 27 09.55	8 16 58.1	215
4780	19.52	1.95	971	45	88	11	0.2	12 27 20.79	8 17 00.9	86
4959	21.38	1.33	1449	44	123	11	-1.3	12 27 23.05	8 17 11.9	
5090	19.83	1.61	582	46	90	-59	-0.6	12 27 09.43	8 17 20.2	218
5323	20.33	0.82	1263 ^a	65	53	-41	-2.5	12 27 16.29	8 17 33.8	130
5456	19.26	1.39	737 ^a	65	68	-66	-1.1	12 27 12.49	8 17 41.4	177
5561	20.82	1.39	903	48	277	-144	-1.1	12 26 56.84	8 17 48.3	
5629	21.09	1.36	522	52	82	-79	-1.2	12 27 11.90	8 17 52.2	
6164	19.79	1.65	426	30	110	-110	-0.5	12 27 12.25	8 18 27.1	181
6231	20.77	1.81	1069 ^a	65	110	-95	-0.1	12 27 16.54	8 18 32.3	127
6284	19.44	1.57	569	54	191	-59	-0.7	12 27 25.39	8 18 36.8	40
6294	21.02	1.64	1034	84	233	-170	-0.5	12 27 01.30	8 18 37.7	
6427	21.11	1.79	1141	50	128	-128	-0.2	12 27 12.47	8 18 47.5	
6520	20.06	1.86	607	57	131	-114	0.0	12 27 16.75	8 18 53.5	121
6564	20.03	1.34	1077	31	147	-146	-1.2	12 27 10.77	8 18 57.2	206
6696	20.08	1.59	550	52	173	-107	-0.6	12 27 21.45	8 19 08.5	82
6721	21.09	1.73	1180	45	185	-174	-0.3	12 27 07.36	8 19 10.5	
6872	20.15	1.46	870	41	178	-175	-1.0	12 27 09.21	8 19 20.7	221
6989	20.61	1.75	1071	50	196	-126	-0.3	12 27 21.98	8 19 30.5	
7197	20.94	1.50	782	50	208	-205	-0.9	12 27 08.44	8 19 48.2	
7340	20.91	1.77	1308	124	197	-173	-0.2	12 27 17.39	8 19 59.0	
7399	20.35	1.40	1005	44	285	-253	-1.1	12 27 01.33	8 20 05.1	
7458	20.75	1.84	807	57	208	-207	-0.1	12 27 12.23	8 20 08.6	
7659	19.87	1.34	1571	56	229	-229	-1.2	12 27 10.54	8 20 24.0	
7784	19.20	1.52	868	51	260	-181	-0.8	12 27 23.22	8 20 34.4	
7889	18.84	1.58	614 ^a	65	285	-179	-0.7	12 27 25.49	8 20 43.5	I-20
7894	21.61	1.73	730	81	302	-281	-0.3	12 27 01.99	8 20 37.2	
7938	20.92	1.44	1251	50	247	-245	-1.0	12 27 11.90	8 20 47.7	

Table 3—Continued

8090	20.51	1.46	903	66	258	-252	-0.9	12 27 13.14	8 21 00.9
8165	20.22	1.39	1027	47	291	-210	-1.1	12 27 23.57	8 21 06.8
8353	20.03	1.98	928	40	293	-293	0.3	12 27 08.71	8 21 22.8
8384	21.39	1.41	768	54	280	-265	-1.1	12 27 15.30	8 21 24.4
8890	20.41	1.88	870	65	329	-309	0.0	12 27 15.77	8 22 14.0
9991	19.41:	1.27:	1040 ^a	65	213	175	-1.4	12 27 26.38	8 14 35.4
9992	19.99:	1.47:	641 ^a	65	34	-27	-0.9	12 27 15.80	8 17 16.7
									34
									135

^aVelocity from Mould *et al.* (1990)

Table 4. Results from non-linear fits of equation 1 to globular cluster samples taken from Table 3. Column 4 contains the confidence level in V_{rot} obtained by randomizing the position angles of the observed clusters. Column 5 contains the 2σ (95% confidence) upper limits to the rotation velocity obtained from Monte-Carlo simulations. The values of V_{rot} in parentheses are those obtained when the position angle of the line of nodes is held fixed at PA= 162 deg.

	V_{rot} (kms $^{-1}$)	θ_0 (deg)	V_0 (kms $^{-1}$)	Confidence (%)	V_{rot}^{max} (95%) (kms $^{-1}$)
All clusters (N=57)	85 (71)	125	970	88	150
Excluding #19 (N=56)	67 (45)	112	956	78	150
Blue clusters (N=30)	159 (142)	131	1038	99	225
Excluding #19 (N=29)	117 (92)	122	1010	96	175
Red clusters (N=27)	50 (7)	83	917	28	100

REFERENCES

Allington-Smith, J.R., Breare, M., Ellis, R.S., Gellatly, D., Glazebrook, K., Jorden, P., Maclean, J., Oates, A.P., Shaw, G., Tanvir, N., Taylor, K., Taylor, P., Webster, J., Worswick, S. 1994, PASP, 106, 983.

Arimoto, N., & Yoshii, Y. 1987, A&A, 173, 23.

Ashman, K.M., Bird, C.M. & Zepf, S.E. 1994, AJ, 108, 2348.

Ashman, K. M. & Zepf, S. E. 1992, ApJ, 384, 50.

Ashman, K.M. & Zepf, S.E. 1997, *Globular Cluster Systems*, Cambridge University Press.

Bird, C.M. & Beers, T.C. 1993, AJ, 105, 1596.

Bridges, T.J., Ashman, K.M., Zepf, S.E., Carter, D., Hanes, D.A., Sharples, R.M. & Kavelaars, J.J. 1997, MNRAS, 284, 376.

Ciardullo, R., Jacoby, G.H. & Dejonghe, H.B. 1993, ApJ, 414, 454.

Cohen, J.G. & Rhyzov, A. 1997, ApJ, 486, 230.

Cole, S., Aragon-Salamanca, A., Frenk, C.S., Navarro, J. & Zepf, S.E. 1994, MNRAS, 271, 781.

Fisher, D., Franx, M. & Illingworth, G. 1995, ApJ, 448, 119.

Forbes, D.A., Brodie, J.P. & Grillmair, C.J. 1997, AJ, 113, 1652.

Geisler, D., Lee, M.G. & Kim, E. 1996, AJ, 111, 1529.

Geisler, D. 1996, AJ, 111, 480.

Grillmair, C.J., Freeman, K.C., Bicknell, G.V., Carter, D., Couch, W.J., Sommer-Larsen, J., Taylor, K., 1994, ApJ, 422, L9.

Harris, W.E., 1991, ARA&A, 29, 543.

Heisler, J., Tremaine, S., Bahcall, J.N., 1985, ApJ, 298, 8.

Hernquist, L. 1993, ApJ, 409, 548.

Hesser, J.E., Shawl, S.J. & Meyer, J.E. 1986, PASP, 98, 403.

Heyl, J.S., Hernquist, L. & Spergel, D.N. 1996, ApJ, 463, 69.

Irwin, J.A. & Sarazin, C.L. 1996, *ApJ*, 471, 683.

Kauffmann, G. 1996, *MNRAS*, 281, 487.

Lee, M.G., Kim, E. & Geisler, D. 1998, *AJ*, in press.

Mould, J.R., Oke, J.B., de Zeeuw, P.T., Nemec, J.M., 1990, *AJ*, 99, 1823.

Nulsen, P.E.J. & Bohringer, H. 1995, *MNRAS*, 274, 1093.

Saglia, R.P., Bertin, G., Bertola, F., Danziger, J., DeJonghe, H., Sadler, E.M., Stiavelli, M., DeZeeuw, P.T. & Zeilinger, W.W. 1993, *ApJ*, 403, 567.

Sandage, A., Tammann, G.A., 1981, *A Revised Shapley-Ames Catalog of Bright Galaxies*, Carnegie Institution.

de Vaucouleurs, G., de Vaucouleurs, A., Corwin, H.G., Buta, R., Paturel, G. & Fouqué, P., 1991, *Third Reference Catalogue of Bright Galaxies*, Springer, New York.

Whitmore, B.C., Sparks, W.B., Lucas, R.A., Machetto, F.D. & Biretta, J.A. 1995, *ApJ*, 454, L73.

Zepf, S.E., Ashman, K.M., 1993, *MNRAS*, 264, 611.

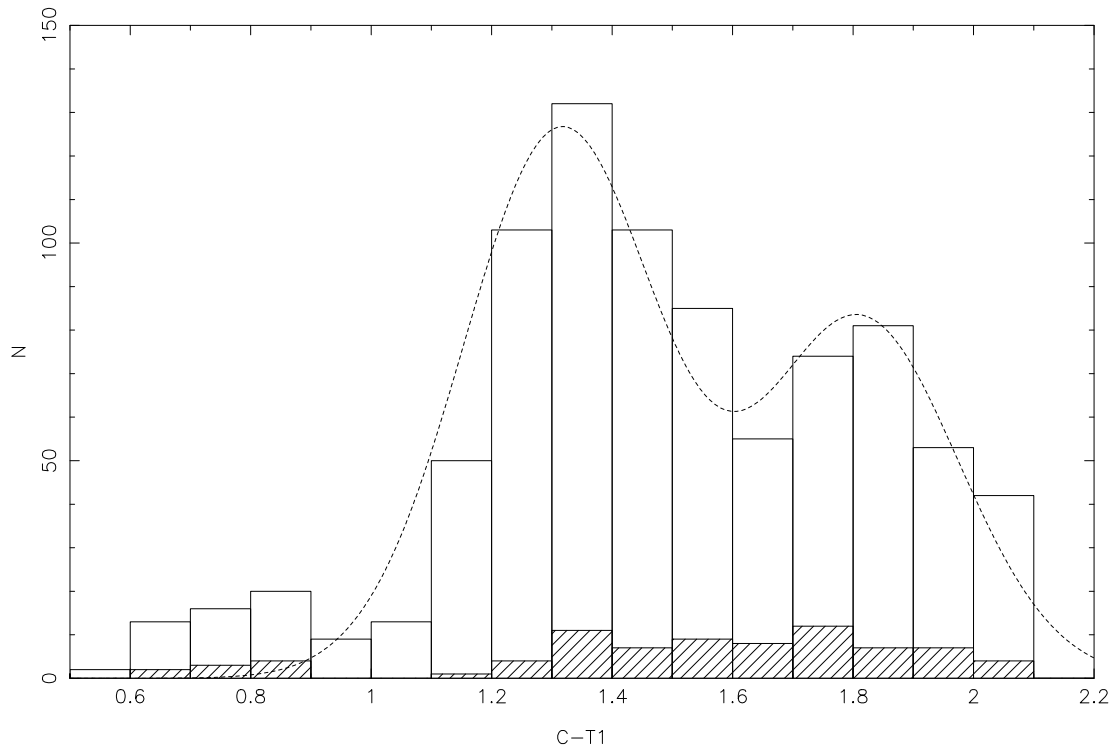


Fig. 1.— Colour distribution for globular cluster candidates with $19.5 < V < 22.5$ and $0.5 < C - T_1 < 2.2$ from Geisler *et al.* (1996). The open histogram is for the full sample of 860 candidates from which our spectroscopic targets were selected; the shaded histogram is for the 79 objects for which spectra were obtained.

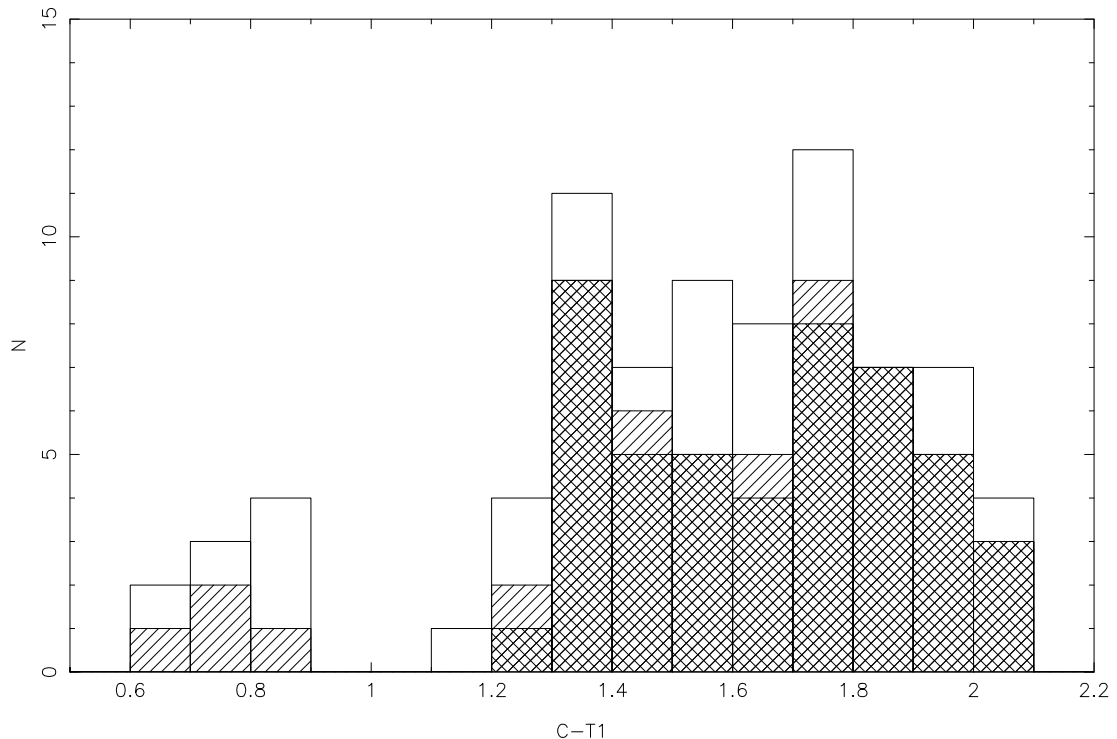


Fig. 2.— The open histogram shows the colour distribution for the 79 globular cluster candidates for which spectra were obtained. The shaded histogram shows the 55 candidates for which reliable velocities were derived from the cross-correlation analysis. The cross-hatched area shows the colour distribution of the 47 objects identified as clusters on the basis of their radial velocities in Table 2.

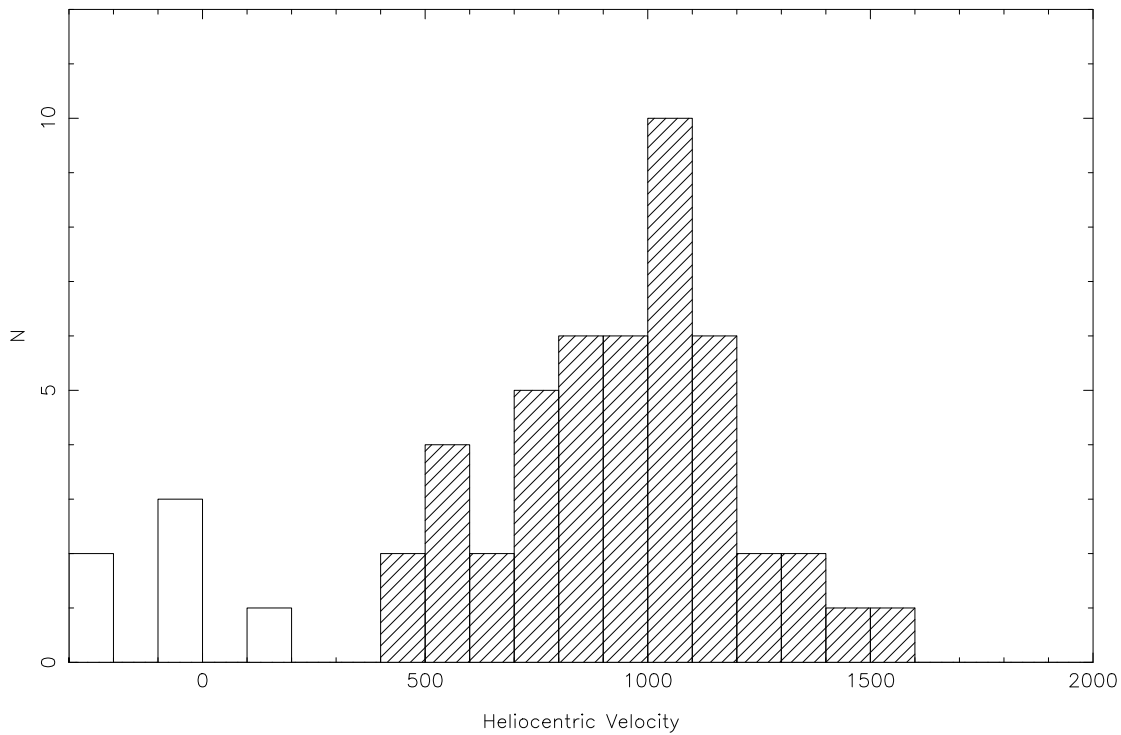


Fig. 3.— Heliocentric velocities for 53 globular cluster candidates around NGC 4472. Two objects (presumably compact galaxies) with velocities > 10000 km s $^{-1}$ have been omitted. The shaded histogram shows those candidates assumed to be bona fide clusters belonging to NGC 4472 (see text for details).

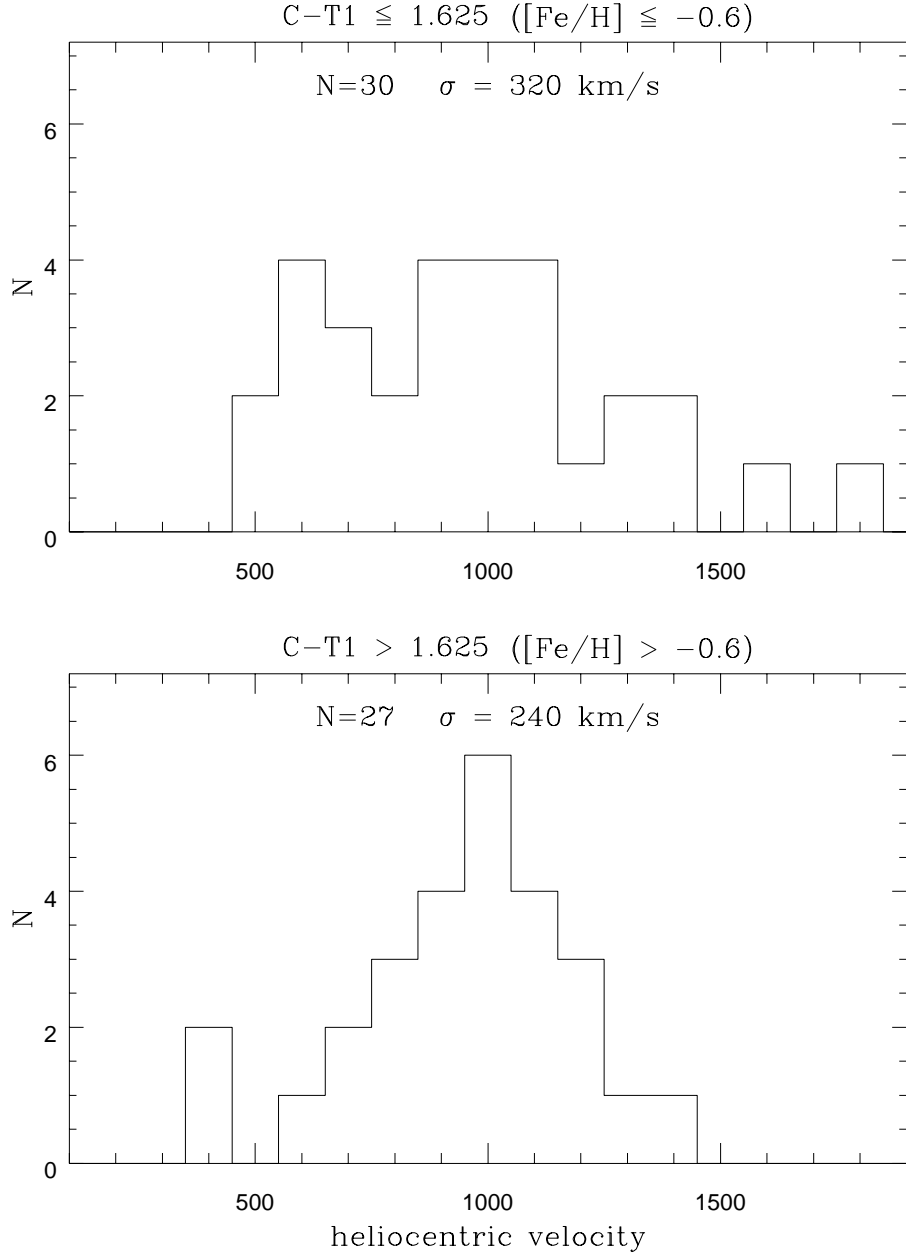


Fig. 4.— A comparison of the velocity distributions of the metal-poor and metal-rich cluster populations in NGC 4472. An F-test rejects the hypothesis that these two have the same dispersion at the 86% confidence level. The mean velocities of the two populations 969 ± 58 km s^{-1} ($N=30$) and 946 ± 46 km s^{-1} ($N=27$) are identical to within the errors.

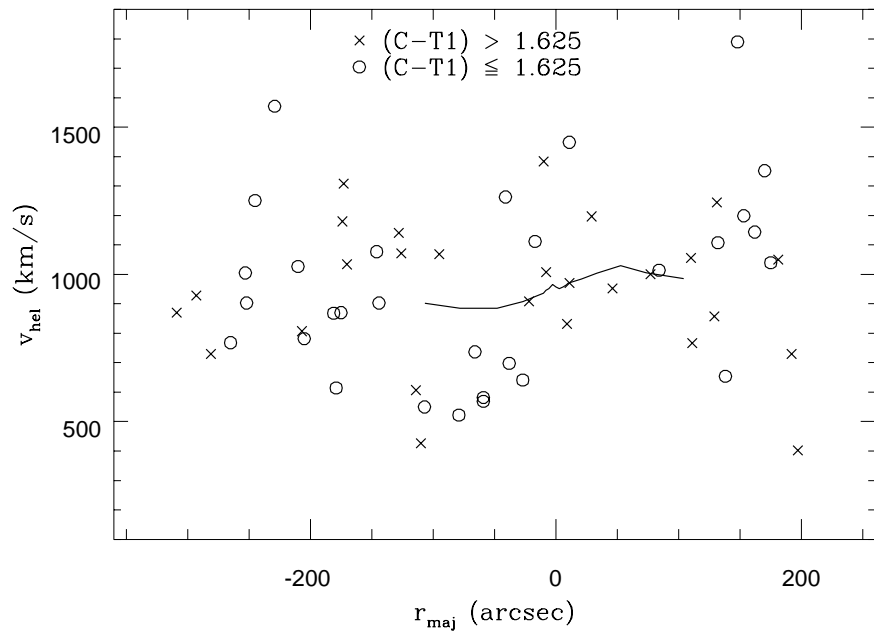


Fig. 5.— A plot of the velocities of globular clusters against their distance projected along the major axis of NGC 4472. The solid line shows the rotation of the stellar component of the galaxy from Fisher *et al.* (1995) normalized to the systemic velocity of the galaxy from Sandage & Tamman (1981).

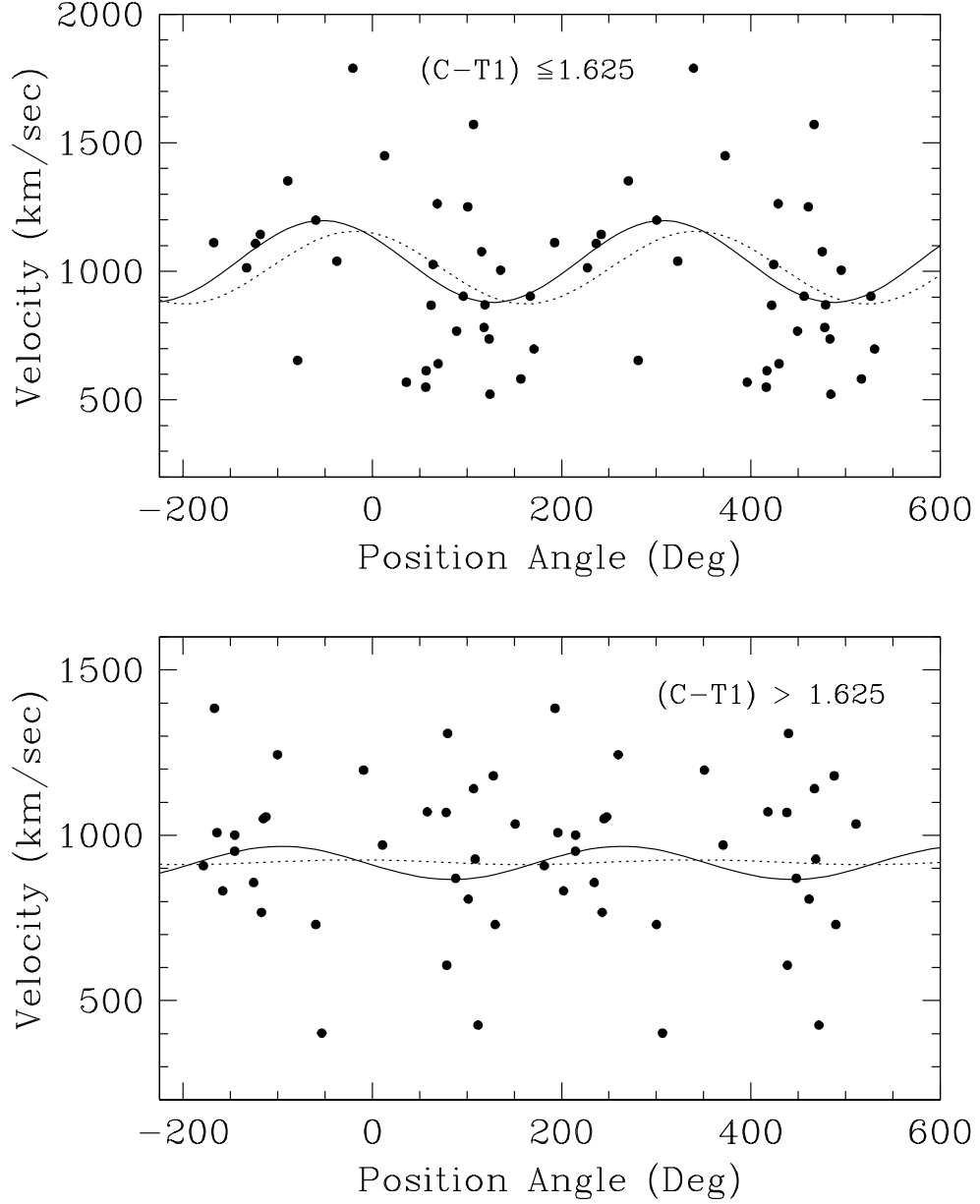


Fig. 6.— A plot of the velocities of globular clusters against their position angle (measured N through E). The major axis of NGC 4472 is at $PA = 162^\circ$ and two complete phases are shown for clarity. The upper panel shows the results for the metal-poor ($C-T_1 \leq 1.625$) clusters; the lower panel shows the metal-rich ($C-T_1 > 1.625$) clusters. Non-linear least squares fits of equation 1 are shown by the solid lines; the dashed lines show the best fit if the position angle is constrained to be 162° .

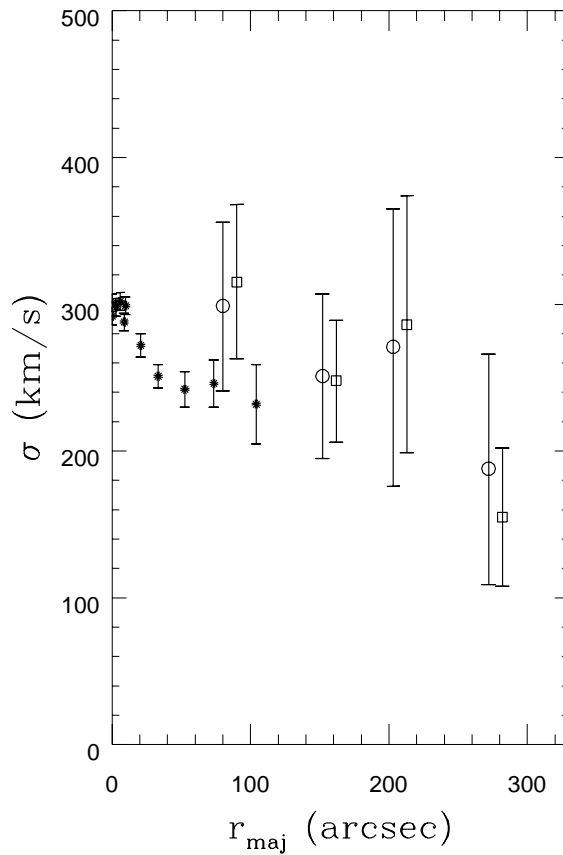


Fig. 7.— A plot of the velocity dispersion of the globular clusters in NGC 4472 against the projected distance along the major axis. Open circles are for the full sample, whilst open squares are excluding cluster # 19. The velocity dispersion of the stellar light is shown by the solid symbols. The importance of globular cluster samples in probing the outer haloes of ellipticals is clearly shown in this plot.

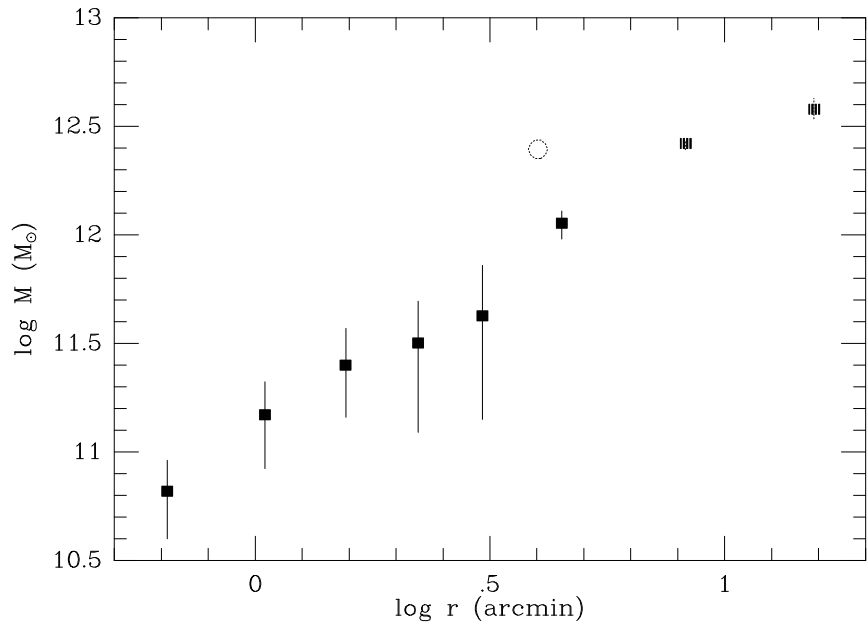


Fig. 8.— Integrated mass distribution for NGC 4472. The solid symbols (with error bars) are the X-ray estimates from Irwin & Sarazin (1986). The open circle shows the projected mass estimator applied to the globular cluster population. All mass estimates have been scaled to a Virgo cluster distance of 16 Mpc.